TECHNICAL ARTICLE

Numerical Simulation of Residence Time Distribution (RTD) in Tundish with Channel Type Induction Heating

BIN YANG [ORCID],[1] XIANGWEI LIAO,[2,3,4] KUN LIU,[1] CHENGLIN ZHAO,[2,3] and PENG HAN[1]

1.—School of Materials and Metallurgy, University of Science and Technology Liaoning, Anshan 114051, People's Republic of China. 2.—State Key Laboratory of Marine Equipment and Applications, Anshan 114009, China. 3.—Ansteel Iron and Steel Research Institute, Anshan 114009, China. 4.—e-mail: 13050097509@163.com

Numerical simulation is an effective tool to analyze complex metallurgical multiphase flow problems especially when the high-temperature melt experiment cannot be carried out. Therefore, a three-dimensional mathematical model has been applied to investigate the fluid flow characteristic of molten steel in a tundish with channel type induction heating. The results show that the thermal buoyancy can increase the mean residence time of molten steel and decrease the dead zone fraction in the tundish with channel induction heating, although the electromagnetic force can increase the dead zone fraction, but it also increases the mixed zone fraction; the mixing of melt benefits inclusion collision-coalescence and removal. The electromagnetic force also can stir the molten steel, completely mixing it in a short time. The main flow behavior is well mixed flow; the secondary flow is plug flow in the tundish with channel-type induction heating.

INTRODUCTION

The tundish is an intermediate reactor between the ladle and the mold, used to become a multifunction vessel.[1–4] Its metallurgical operations such as inclusion removal,[5–12] temperature compensation,[13–17] alloy trimming,[1,18] and thermal and particulate homogenization are important for clean molten steel. The main currents of the presented studies concern physical experiments and numerical simulation of the melt flow phenomena and refining processes.[19]

For the conventional tundish, inclusion removal rate can be an indispensable evaluation target to judge the quality of molten steel, its collision-coalescence, growth, and removal process depending on the flow condition of molten steel. Research shows that fluid flow characteristics dominate the particle motion, heat transfer, and homogenization in most heteromorphic tundish. Therefore, it is necessary to analyze its fluid-dynamic behavior and thus make a suitable design or optimize the control devices (dams, baffles, weirs, turbulence inhibitors, gas curtains, etc.) to obtain the most favorable conditions to produce high-quality clean steel.[20–25] A commonly used ideal in improving the use of internal flow space of steel of a tundish is also to combine the different flow control devices.[20–25] Therefore, the design, operating parameters, source fields (bubble or electromagnetic force), and macroscopic transport behavior of physical systems must be optimized to ensure sufficient residence time and to produce suitable metal flow patterns.[26–28] Based on the above, the molten steel flow in the tundish has been widely studied by a concept residence time distribution (RTD);[29–31] research output in this field can be found in previous reports or literature and is methodologically diverse. RTD in physical experiments or numerical simulation is used to characterize the fluid flow state.

For the conventional tundish, control flow devices can change the melt flow effectively. Its design and optimization is relatively easy because of the vast interior space of tundish. The melt flow condition is

easy to obtain through the RTD. Then, the dead zone, plug zone, and well-mixed zone in a given tundish can be readily estimated in detail. The RTD characteristics are applied to compare tundish with diverse geometric shapes, control flow equipment, and working operations. The details of flow can be obtained from a whole tundish. Generally speaking,, an appropriate tracer is injected into the fluid from the ladle shroud, and the concentration of added tracer is monitored dynamically at the exit nozzle of the tundish.[1]

At present, the function of the tundish with channel induction heating is to improve the super-heat and inclusion removal. Previous studies of the tundish focused on the electromagnetic, flow, temperature, and inclusion fields. It is necessary to analyze and investigate the desired characteristics for transport behavior in the tundish with channel induction heating. In the current work, an attempt was made to use numerical simulation to unveil the flow characteristics through the RTD curves occurring in a tundish with channel induction heating. Investigation of the tundish with electromagnetic force and Joule heat will be different from the optimization or comparison for conventional tundish. Three important points in this paper are: first to investigate the RTD curve of tundish with channel-type induction heating, second to investigate the flow characteristic in the tundish with Joule heat and electromagnetic force, and third to determine the tracer transport behavior in the tundish with channel-type induction heating. The numerical simulations made it possible to evaluate the macroscopic mixed flow of molten steel in the case without induction heating, Joule heat, electromagnetic force, and induction heating.

GEOMETRICAL MODEL

Figure 1 and Table I show the more specific details of structure, size, and operating parameters of the tundish with channel-type induction heating.[11,13] The channel plays two important key roles in the tundish. The first function is to heat the molten steel by Joule heat, which is caused by induced current. The second function is to stir the molten steel by electromagnetic force, which is caused by the interaction between the induced current field and magnetic field.[14]

MATHEMATIC MODELS

The electromagnetic field, fluid flow, heat transfer, and tracer transport in the tundish can be described as the following equations.[11,13]

Magnetic field constitutive equation:

$$\nabla\left(\frac{1}{\mu}\nabla\times\vec{A}\right) + \sigma\left(\frac{\partial\vec{A}}{\partial t} + \nabla\varphi\right) = 0 \qquad (1)$$

in molten steel region

$$\nabla\times\left(\frac{1}{\mu}\nabla\times\vec{A}\right) = \vec{J}_s \quad \text{in other regions} \qquad (2)$$

$$\nabla\cdot\vec{A} = 0 \qquad (3)$$

Continuity equation:

$$\frac{\partial\rho_f}{\partial t} + \nabla\cdot(\rho_f\vec{u}_f) = 0 \qquad (4)$$

Momentum equation:

$$\frac{\partial(\rho_f\vec{u}_f)}{\partial t} + \nabla\cdot\left(\rho_f\vec{u}_f\vec{u}_f\right) = -\nabla P + \rho_f\vec{g} + \beta(T_0-T)\rho_f\vec{g}$$
$$+ \nabla\cdot\left[\mu_{\text{eff}}\left(\nabla\vec{u}_f + \left(\nabla\vec{u}_f\right)^T\right)\right]$$
$$+ \vec{J}\times\vec{B} \qquad (5)$$

Turbulent kinetic energy and rate of dissipation:

$$\frac{\partial(\rho_f\kappa)}{\partial t} + \frac{\partial(\rho_f\kappa\vec{u}_f)}{\partial x_j} = \frac{\partial}{\partial x_j}\left[\left(\mu+\frac{u_t}{\sigma_k}\right)\frac{\partial\kappa}{\partial x_j}\right] + G_k - \rho_f\varepsilon \qquad (6)$$

$$\frac{\partial(\rho_f\varepsilon)}{\partial t} + \frac{\partial(\rho_f\varepsilon u_j)}{\partial x_j} = \frac{\partial}{\partial x_j}\left[\left(\mu+\frac{u_t}{\sigma_\varepsilon}\right)\frac{\partial\varepsilon}{\partial x_j}\right] + \frac{C_{1\varepsilon}\varepsilon}{\kappa}G_\kappa$$
$$- C_{2\varepsilon}\rho_f\frac{\varepsilon^2}{\kappa} \qquad (7)$$

Energy conservation equation:

$$\frac{\partial(\rho c_P T)}{\partial t} + \nabla\cdot\left(\rho_f T\vec{u}\right) = \nabla\cdot(\lambda\nabla T) + \sigma J^2 \qquad (8)$$

Tracer transport equation:

$$\frac{\partial(\rho_f C)}{\partial t} + \nabla\cdot\left(\rho_f\vec{u}_f C\right) = \nabla\cdot(D_{\text{eff}}\cdot\nabla C) \qquad (9)$$

where $\vec{A}$ is the magnetic vector potential, ϕ is the electric scalar potential, σ is the electrical conductivity, $\vec{J}_s$ is the source current, μ is the magnetic conductivity, μ_{eff} is the effective viscosity, ρ_f is the fluid density, $\vec{u}_f$ is the fluid velocity, P is the pressure, $\vec{g}$ is the gravitational accelerate, κ is the turbulence kinetic energy, ε is the turbulent kinetic energy rate, σ_κ and σ_ε represent the Schmidt number for κ and ε, G_k is the generation rate of turbulence energy, C_p is the heat capacity, T is the temperature, and C is the mass fraction of the injected tracer.
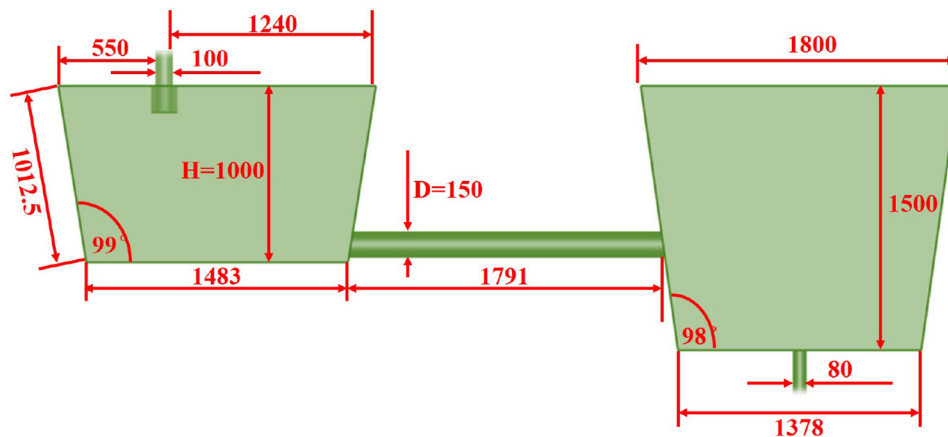
The most widely used analysis models of the RTD (residence time distribution) curve are the classic combined model and the Sahai modified model at
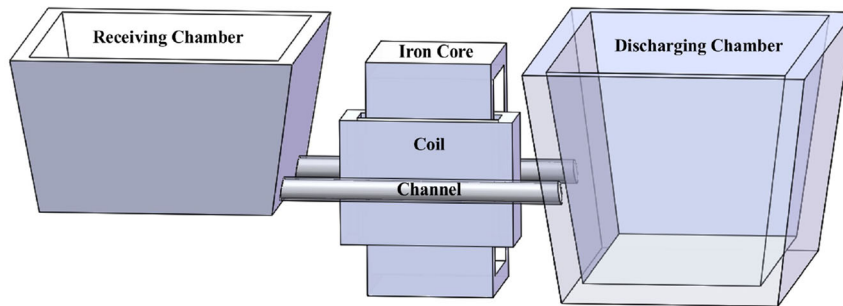
(a) Tundish model
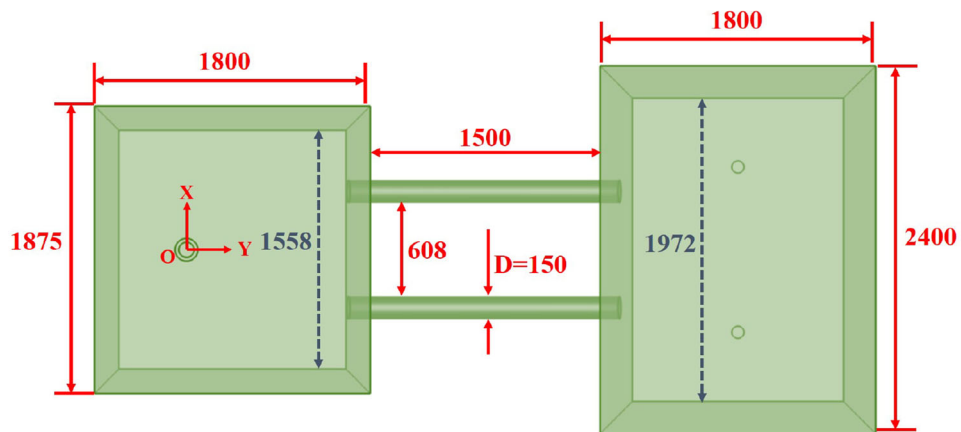
(b) Top view

(c) Front view

Fig. 1. Schematic of tundish with channel-type induction heating (all dimensions are in mm).

present.[32] By comparing the two models, the classic combined model is applied to calculate the plug, the well-mixed, and the dead zones of the tundish.

The classic combined model is applied to calculate the plug zone fraction (V_{pv}), the well-mixed zone fraction (V_{mv}), and the dead zone fraction (V_{dv}) of the tundish. The C curve is applied to obtain the volume fraction; the calculation formula is

Table I. Operating, geometry, and physical parameters of computational models

Parameters	Value	Units
Volumetric flow rate at the ladle shroud	14	m^3/h
Volume of receiving chamber	2.826	m^3
Volume of channel	0.062	m^3
Volume of discharging chamber	5.243	m^3
Relative permeability of molten steel	1	–
Relative permeability of iron core	1000	–
Resistivity of molten steel	1.4×10^{-6}	Ω·m
Relative permeability of copper coil	1	–
Relative permeability of air	1	–
Thermal conductivity of molten steel	41	(W/(m·K))
Heat capacity of molten steel	750	(J/(kg·K))
Relative permeability of molten steel	1	–
Relative permeability of iron core	1000	–
Temperature of ladle shroud	1800	K
Schmidt number	1	–

Table II. Heat losses from the tundish

Parameter	Value (W/m^2)
Free surface heat loss	8000
Bottom heat loss	1800
Wide wall heat loss	4000
Narrow wall heat loss	4200
Channel wall heat loss	1100

$$V_{\mathrm{dv}} = 1 - \frac{t_{\mathrm{av}}}{t_s} \qquad (10)$$

$$V_{\mathrm{pv}} = \frac{t_{\min} + t_{\max}}{2t_0} \qquad (11)$$

$$V_{\mathrm{mv}} = 1 - V_{\mathrm{dv}} - V_{\mathrm{pv}} \qquad (12)$$

where the t_{av} is the mean residence time, t_0 is the theoretical residence time, $t_{\min}$ is the minimum residence time, $t_{\max}$ is the peak concentration time, V_{mv} is the volume fraction of well-mixed zone, V_{dv} is the volume fraction of dead zone, and V_{pv} is the volume fraction of plug zone.

MODEL ASSUMPTIONS

(1) The iron core is isotropic, and its electromagnetic properties are constant.
(2) The effect of fluid flow on the electromagnetic field is too weak to be neglected.
(3) The fluid flow in the tundish is steady and incompressible turbulent flow.
(4) There is no chemical reaction in the tundish.
(5) The tracer has the same physical parameter as the fluid in the tundish.
(6) The free surface is flat in the tundish.

Boundary Conditions

Electromagnetic field and flux parallel boundary conditions are imposed on the exterior surface of the computational domain. The low field, with four types of boundaries, encloses the domain: the inlet, outlet, free surface, and solid wall. The symmetry condition is applied at the free surface, and the wall function method is applied near the wall. For the temperature field, there are also four types of boundaries, the inlet, outlet, free surface, and tundish wall. Table II shows the heat flux at the free surface and the tundish walls. For the tracer transfer, a zero gradient or flux boundary condition was applied for the tracer concentration on the walls, free surface, and outlets for the tracer dispersion equation.

Numerical Solution and Convergence Criteria

The governing equations are solved by the commercial software package CFX and ANSYS-EMAG module (version 11.0, ANSYS, Pittsburgh, PA, USA), which is based on the finite volume method and finite element method. The calculation domain is covered by about 300,000 hexahedral grids. The fluid flow model and the heat transport model are coupled to obtain the flow field and the temperature field, based on the known flow field; the tracer transport equation is solved to obtain the RTD curve. During iteration, the convergence was assumed to reach a point where all the normalized residuals are $< 10^{-5}$.

RESULTS AND DISCUSSION

Grid Independence

The grid system consists of 196,156, 248,300, 300,318, 324,848, and 350,580 grids, which are applied to ensure the accuracy and reliability of the numerical result. Table III gives the related

Table III. Analysis result of velocity for different grid numbers

Grid numbers	196,156	248,300	300,318	324,848	350,580
Test point	K	K	K	K	K
Velocity (m/s)	0.125271	0.126333	0.126674	0.1258324	0.125795

Table IV. Analysis results in the tundish for water model and numerical simulation

Cases	V_{pv} (%)	V_{dV} (%)	V_{mv} (%)
Numerical calculation	33.05	9.55	57.40
Water model	33.72	9.48	56.80

analysis result of test point K. From the mesh 196,156 to 350,580, the variation of velocity value is on the third digit (the maximum related error is only 1.12%). Therefore, the 300,318 mesh can be applied to obtain the RTD curves.

Model Validation

Figure 2 and Table IV give the RTD curve and the fluid flow characteristic in the water model and simulation calculation. The measured values of volume fraction are 33.72%, 9.48%, and 56.8%,
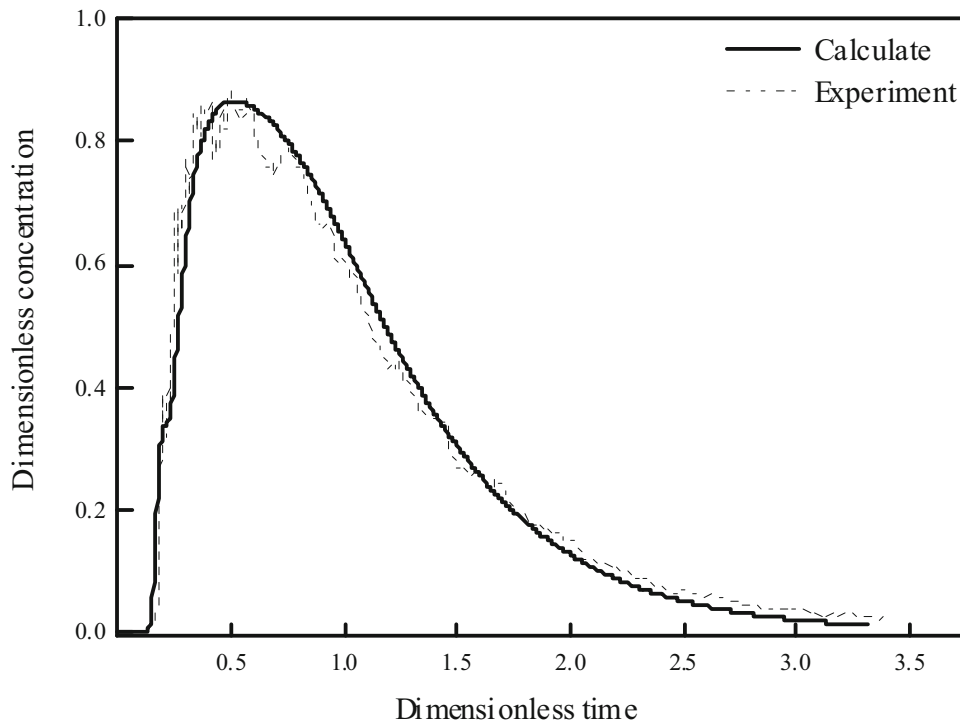

Fig. 2. RTD curve in the tundish for water model and numerical simulation.

Table V. Four cases in the numerical simulation

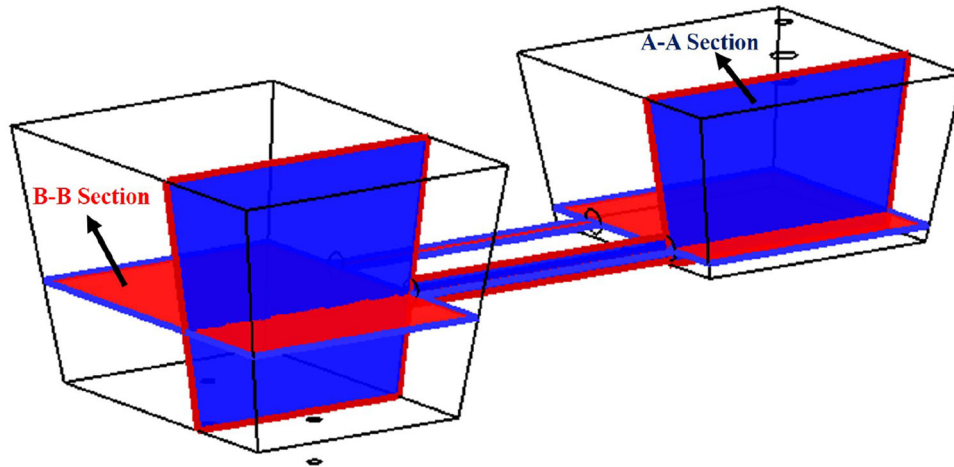| Cases	Source terms	Metallurgical effect
Case 1	No	No channel induction heating
Case 2	Joule heat	Thermal buoyancy
Case 3	Electromagnetic force	Stirring effect
Case 4	Electromagnetic force + Joule heat	Channel induction heating

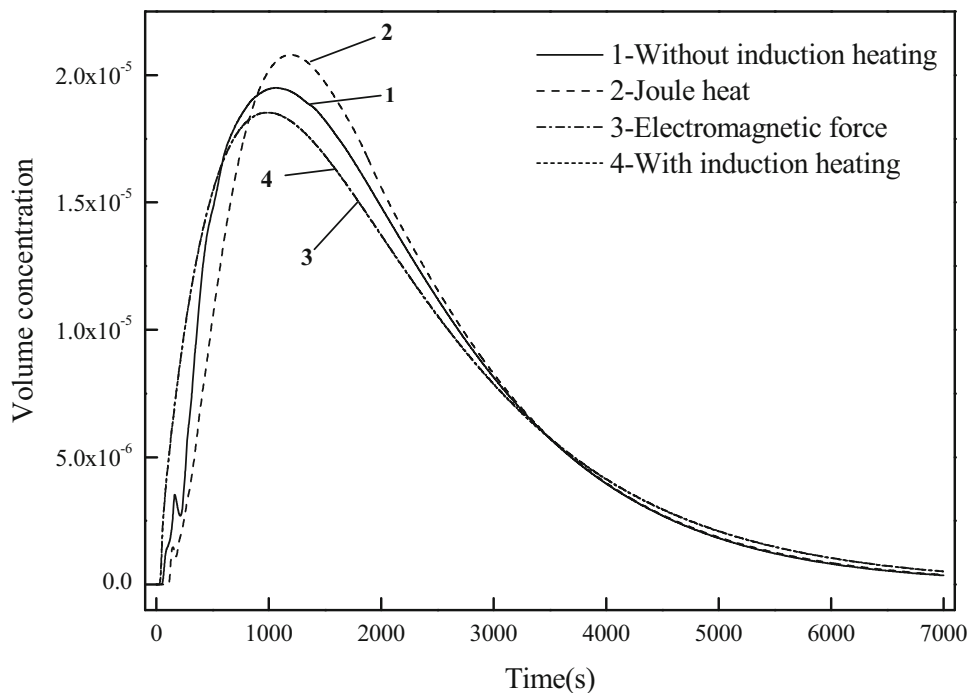Fig. 3. Characteristic sections in the tundish.

Fig. 4. RTD curves in the tundish for four cases.

and the predicted results are 33.05%, 9.55%, and 57.40%. The related errors are only 2.03%, 0.75%, and 1.78%, respectively, between the predicted and measured results; the relative error is $< 5\%$, and the predicted result agrees with the experimental data of the water model. The difference between the predicted curve and the experimental curve comes from several factors. (1) In the experiment, the tracer has solute buoyancy in water, but the mathematical model ignores the solute. (2) The fluid flow in the water model is turbulent, which is anisotropic, while in the mathematical model, the fluid flow is isotropic fluid. (3) The oscillating free surface

in the water model has an impact on curves, while it is assumed to be flat in the mathematical model.

Analysis of RTD

Electromagnetic force and Joule heat are two key characteristics of a tundish with channel type induction heating. Therefore, the influence of electromagnetic force and Joule heat on the macroscopic mixed flow of fluid needs to be deeply studied.

To determine the details about the effect of the source field (electromagnetic field and Joule heat field) on RTD (residence time distribution) in a tundish with channel induction heating, the
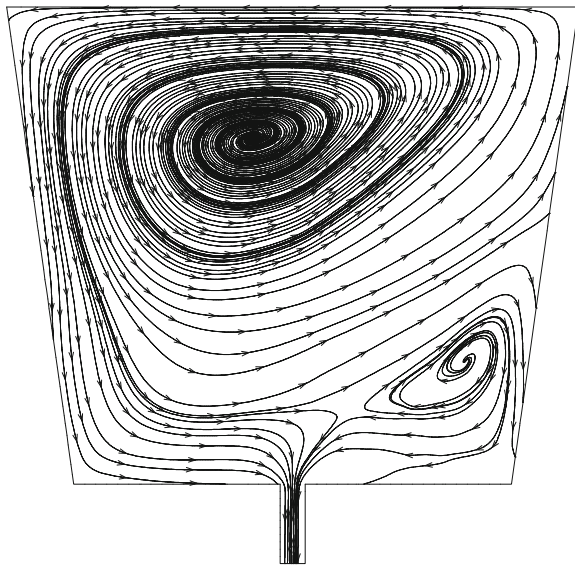
(a) Without electromagnetic force
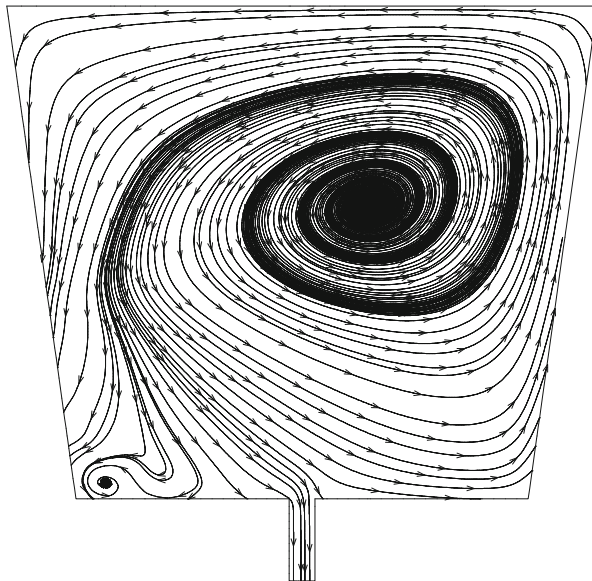
(b) With electromagnetic force

Fig. 5. Outlet cross section of tundish in the receiving chamber.

calculation is divided into four cases, shown in Table V. Case 1 is the tundish without channel induction heating. Case 2 needs to solve the energy equation with Joule heat. Case 3 needs to solve the momentum equation with electromagnetic force, and the Case 4 needs to solve the energy equation with Joule and the momentum equation with electromagnetic force.

To describe the spatial distribution of fluid flow and tracer concentration in the tundish clearly, some characteristic cross sections need to be defined, as shown in Fig. 3. Section A-A and section B-B pass through the center axis of the channel.

Figure 4 gives the RTD curve in the tundish with channel induction heating under four conditions (without induction heating, Joule heat, electromagnetic force, and induction heating). The curve shows some interesting features. (1) In the case without induction heating and Joule heat, the double peak phenomena appeared in the RTD curve. This is due to the obvious presence of the double-vortex phenomenon in the receiving chamber, as shown in the Fig. 5a. (2) In the case of electromagnetic force and channel induction heating, the double-peak phenomena do not appear in the RTD curve. This is because there is a big and a small recirculation zone in the receiving chamber, but the smaller counterclockwise vortex has little influence on tracer transport at the lower left corner, and the larger counterclockwise recirculation zone leads to a homogeneous mixing of the tracer, as shown in Fig. 5b. The two RTD curves basically coincide in shape; this is because the electromagnetic force has a larger driving force than Joule heat. As a result, the Joule heat can be ignored under the strong electromagnetic force. (3) The sequence of the peak concentration from small to large for the different cases is: Case 4 → Case 3 → Case 1 → Case 2. This is because the electromagnetic force increases the mixed effect of molten steel in the whole tundish; meanwhile, the rapid flow of molten steel in the tundish leads to premature peak concentration. In the case of Joule heat, due to the high temperature, molten steel flows from the channel to receiving chamber; the fluid flows upward and extends the flow trajectory of fluid in the receiving chamber.

Table VI. Fluid flow characteristics in the tundish with channel induction heating for different type of cases

Cases	Residence time(s)				Volume fraction (%)		
	$t_{\min}$	$t_{\max}$	t_{av}	t_s	V_{pv}	V_{mv}	V_{dv}
Case1	76	1065	1850.1	2070.5	27.6	61.8	10.6
Case2	131	1194	1904.9	2070.5	32.0	60.0	8.0
Case3	44	991	1813.7	2070.5	25.0	62.6	12.4
Case4	44	990	1812.1	2070.5	25.0	62.6	12.4

(a) Without channel induction heating

(b) Thermal buoyancy

(c) Stirring effect

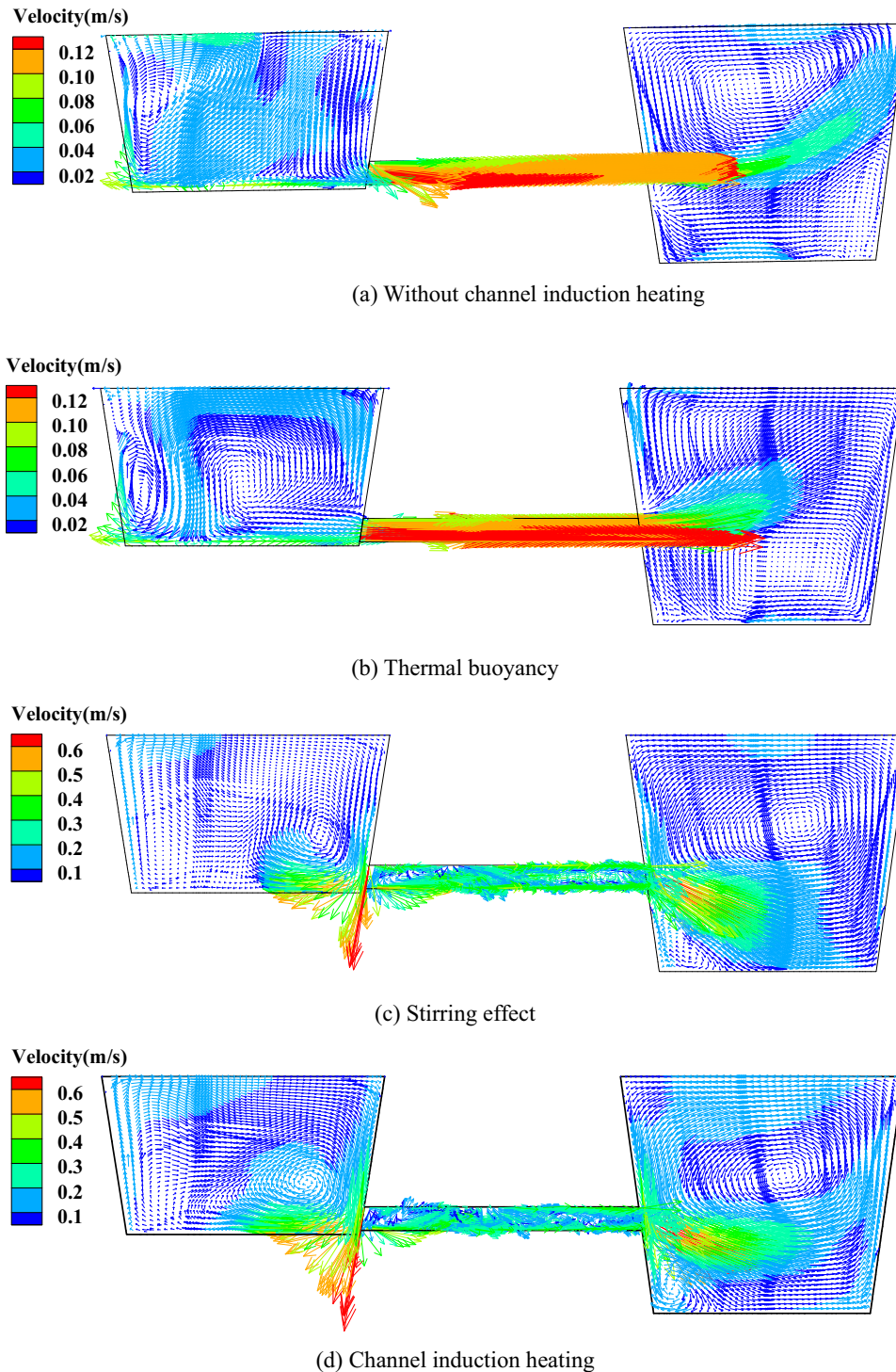
(d) Channel induction heating

Fig. 6. Velocity field in the tundish at A-A section.

Therefore, the residence time of molten steel increases greatly in the receiving chamber.

Table VI gives the flow characteristic of molten steel for the different types of cases. It shows that:

(1) The sequence of the mean residence time of molten steel from small to large for the different cases is: Case 4 → Case 3 → Case 1 → Case 2 (1812.1 s < 1813.7 s < 1850.1 s < 1904.9 s). Case 2 demonstrates a longer mean residence time compared to Case 1, 3 and 4; this is because there are two recirculation zones in the discharging chamber. One small recirculation is on the left side and another large recirculation is in the middle area, and there is a large recirculation zone in the lower

region in the receiving chamber. The three recirculation zones and velocity of molten steel with no speed difference from the tundish without channel induction heating lead to a longer mean residence time, as shown in Fig. 6a and b. In the case of electromagnetic force and channel induction heating, the residence time of molten steel is shorter. This is because that the velocity of molten steel with electromagnetic force is much greater than that without electromagnetic force. The molten steel flows out of the outlet quickly, as shown in Fig. 6c and d. Therefore, according to the above, the electromagnetic force will shorten the residence time of molten steel in the tundish with channel induction heating.

(2) The sequence of the dead zone fraction from small to large for the different cases are: Case $2 \rightarrow$ Case $1 \rightarrow$ Case 3 = Case 4 (8.0% < 10.6% < 12.4% = 12.4%). Case 3 and Case 4 have longer mean residence time compared to Cases 1 and 2; this is because the electromagnetic force leads to an increasing velocity of molten steel and short residence time of molten steel, and the dead zone is determined by the residence time. On the contrary, the Joule heat leads to a longer residence time of molten steel, resulting in an absolutely natural smaller dead zone.

(3) The sequence of the plug zone fraction from small to large for the different cases are: Case $2 \rightarrow$ Case $1 \rightarrow$ Case 3 = Case 4 (60.0% < 61.8% < 62.6% = 62.6%). Case 3 and Case 4 have longer mean residence time compared to Cases 1 and 2. This is because the magnitude of electromagnetic force is on the order of 10^5 N/m^3, which is greater than the gravity of molten steel 7×10^4 N/m^3, and promotes better stirring of the molten steel by electromagnetic force.[11] Although the Joule heat extends the flow trajectory of molten steel, it decreases the recirculation zone and the mixing effect in the receiving chamber, as shown in Fig. 6b.

(4) The sequence of the minimum residence time of tracer from small to large for the different cases is: Case 4 = Case $3 \rightarrow$ Case $1 \rightarrow$ Case 2 (44 s = 44 s < 76 s < 131 s). The minimum residence time of Case 2 is the largest compared to Cases 1, 3 and 4. The peak concentration of tracer from small to large for different cases are: Case $4 \rightarrow$ Case $3 \rightarrow$ Case $1 \rightarrow$ Case 2 (990 s < 991 s < 1065 s < 1194 s). Two physical quantities conform to the same rule; the electromagnetic force and Joule heat show a different effect on molten steel. Both sources can change the flow behavior, but the former mainly focuses on stirring and the latter mainly on temperature compensation.

CONCLUSION

The following conclusions are summarized as follows:

(1) The predicted RTD curve agrees well with the water model.

(2) The mean residence times of molten steel of 1904.9 s in the tundish with Joule heat are 54.8 s, 91.2 s, and 92.8 s greater than the mean residence time of 1850.1 s, 1813.7 s, and 1812.1 s in the tundish without induction heating, with electromagnetic force and induction heating, respectively.

(3) The thermal buoyancy can increase the mean residence time of molten steel and decrease the dead zone fraction in the tundish with channel type.

(4) The electromagnetic force increases the dead zone fraction, but it increases the mixed zone fraction. The mixing of molten steel benefits inclusion collision-coalescence and growth.

(5) The main flow behavior is well mixed flow; the secondary flow is plug flow in the tundish with channel type induction heating.

ACKNOWLEDGEMENTS

CONFLICT OF INTEREST

The authors declare that there is no conflict of interest.

REFERENCES

1. D. Mazumdar and R.I.L. Guthrie, *ISIJ Int.* 39, 524 (1999).
2. D. Mazumdar, *Steel Res. Int.* 90, 201800279 (2018).
3. Y. Sahai, *Metall. Mater. Trans. B* 47, 2095 (2016).
4. K. Chattopadhyay, M. Issac, and R.I.L. Guthrie, *ISIJ Int.* 50, 331 (2010).
5. S. Joo and R.I.L. Guthrie, *Metall. Trans. B* 24, 755–765 (1993).
6. S. Joo, J.W. Han, and R.I.L. Guthrie, *Metall. Trans. B* 24, 767 (1993).
7. S. Joo, J.W. Han, and R.I.L. Guthrie, *Metall. Trans. B* 24, 779 (1993).
8. L.F. Zhang, S. Taniguchi, and K.K. Cai, *Metall. Mater. Trans. B* 31, 253 (2000).
9. Y. Miki and B.G. Thomas, *Metall. Mater. Trans. B* 30, 639 (1999).
10. B. Yang, H. Lei, Q. Bi, Y.Y. Xiao, and Y. Zhao, *JOM* 70, 2950 (2018).
11. B. Yang, H. Lei, Q. Bi, J.M. Jiang, H.W. Zhang, Y. Zhao, and J.A. Zhou, *Steel Res. Int.* 89, 201800145 (2018).
12. H. Lei, B. Yang, Q. Bi, Y.Y. Xiao, S.F. Chen, and C.Y. Ding, *ISIJ Int.* 59, 1811 (2019).
13. B. Yang, H. Lei, Q. Bi, J.M. Jiang, H.W. Zhang, Y. Zhao, and J.A. Zhou, *Steel Res. Int.* 89, 201800173 (2018).

14. Q. Wang, B.K. Li, and F. Tsukihashi, *ISIJ Int.* 54, 311 (2014).
15. A. Bermudez, D. Gomez, M.C. Muniz, P. Salgado, and R. Vazquez, *Appl. Numer. Math.* 59, 2082 (2009).
16. H.Y. Tang, L.Z. Guo, G.H. Wu, H. Xiao, H.Y. Yao, and J.Q. Zhang, *Metals.* 8, 8060374 (2018).
17. Q. Yue, C.B. Zhang, and X.H. Pei, *Ironmak. Steelmak.* 44, 227 (2017).
18. A. Cwudzinski, *Ironmak. Steelmak.* 42, 132 (2015).
19. T. Merder and M. Warzecha, *Metall. Mater. Trans. B* 43, 856 (2012).
20. R.D. Morales, J.J. Barreto, S. Lopez-Ramirez, J. Palafox-Ramos, and D. Zacharias, *Metall. Mater. Trans. B.* 31, 1505 (2000).
21. S. Lopez-Ramirez, J. Palafox-Ramos, R.D. Morales, J. de Barreto, and D. Zacharias, *Metall. Mater. Trans. B* 32, 615 (2001).
22. S. Chakraborty and Y. Sahai, *Metall. Trans. B* 23, 153 (1992).
23. J. Palafox-Ramos, J.J. Barreto, S. Lopez-Ramirez, and R.D. Morales, *Ironmak. Steelmak.* 28, 1041 (2001).
24. A. Tripathi and S.K. Ajmani, *ISIJ Int.* 45, 1616 (2005).
25. A. Zamora, R.D. Morales, M. Diaz-Cruz, J. Palafox-Ramos, and J.J. Barreto-Sandoval, *Metall. Mater. Trans. B* 35B, 247 (2004).
26. K. Chattopadhyay, M. Isac, and R.I.L. Guthrie, *ISIJ Int.* 51, 573 (2011).
27. S. Chang, X.K. Cao, C.H. Hsin, Z.S. Zou, M. Isac, and R.I.L. Guthrie, *ISIJ Int.* 56, 1188 (2016).
28. Y. Miki, H. Kitaoka, N. Bessho, T. Sakuraya, and M. Kuga, *Tetsu-to- Hagane* 82, 498 (2009).
29. F. Kemeny, D.J. Harris, A. McLean, T.R. Meadowcroft, and J.D. Young, In: *Proc, of the 2nd Process Technology Conf.*, (TMS, Warrendale, PA, 1981) p. 232.
30. Y. Sahai and R. Ahuja, *Ironmak. Steelmak.* 13, 241 (1986).
31. Y. Sahai and T. Emi, *ISIJ Int.* 36, 667 (1996).
32. H. Lei, *Metall. Mater. Trans. B* 46, 2408 (2015).